Assembly-diassembly-organisation-reassembly synthesis of zeolites based on cfi-type layers

Daniel S. Firth[a], Samuel A. Morris[a], Paul S. Wheatley[a], Samantha E. Russell[a], Alexandra M. Z. Slawin[a], Daniel M. Dawson[a], Alvaro Mayoral[b], Maksym Opanasenko[c], Miroslav Polozij[d], Jiři Čejka[c], Petr Nachtigall[d] and Russell E. Morris*[,a,d]

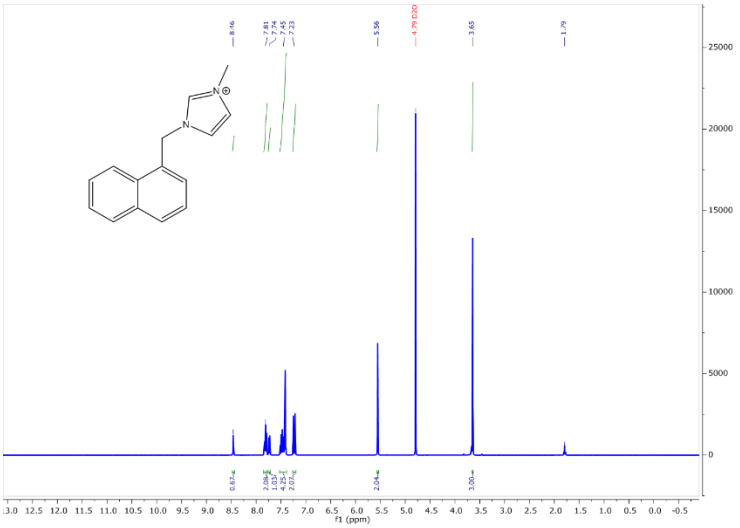

Figure S1. ^{1}H NMR spectrum and the corresponding structure for the priori designed SDA 1-methyl-3-(naphthalen-1-ylmethyl)-imidazolium cation.

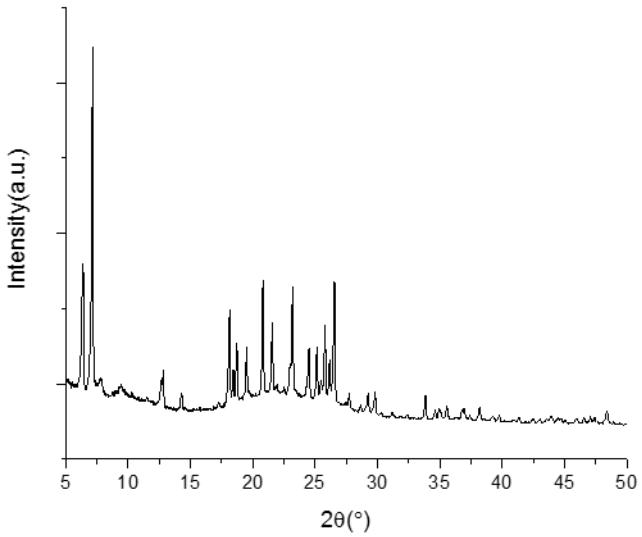

Figure S2. PXRD pattern of SAZ-1, which compared favorably with those obtained for CIT-13 and NUD-2

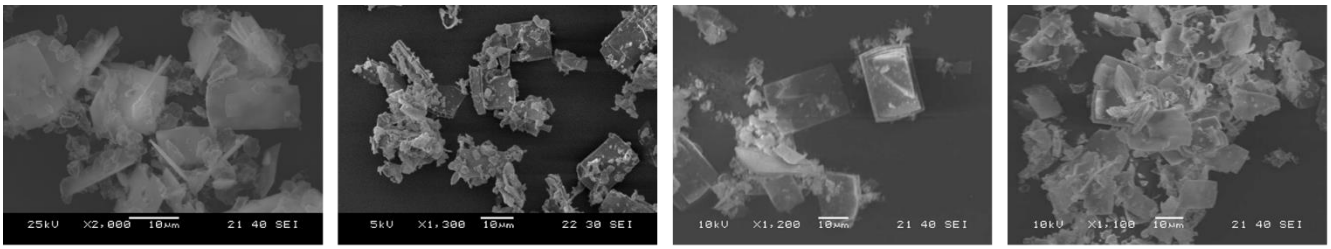

Spectrum	O	Si	Ge	Total
1	70.83	25.35	3.82	100
2	51.65	45.03	3.32	100
2	58.14	38.65	3.21	100
Max.	70.83	45.03	3.82	
Min.	51.65	25.35	3.21	

Spectrum	O	Si	Ge	Total
1	80.01	19.24	0.74	100
2	78.75	20.38	0.87	100
3	78.68	20.41	0.91	100
Max.	80.01	20.41	0.91	
Min.	78.68	19.24	0.74	

Spectrum	O	Si	Ge	Total
1	73.66	25.64	0.7	100
2	68.21	31.15	0.64	100
3	74.72	24.61	0.66	100
Max.	74.72	31.15	0.7	
Min.	68.21	24.61	0.58	

Spectrum	O	Si	Ge	Total
1	70.12	29.09	0.79	100
2	68.24	31.2	0.56	100
3	72.54	26.77	0.69	100
Max.	72.54	33.94	0.79	
Min.	65.31	26.77	0.56	

Fig. S3 SEM images and corresponding EDX analysis of (from left to right) the germanosilicate SAZ-1, hydrolysed SAZ-1 and daughter zeolites IPC-15 and IPC-16. All showing the characteristic rectangular morphology of the parent and daughter zeolites. EDX analysis also confirming the presence of germanium within SAZ-1 and its subsequent removal in hydrolysis and its lack of presence in IPC-15 and IPC-16 (EDX results given in atomic percent).

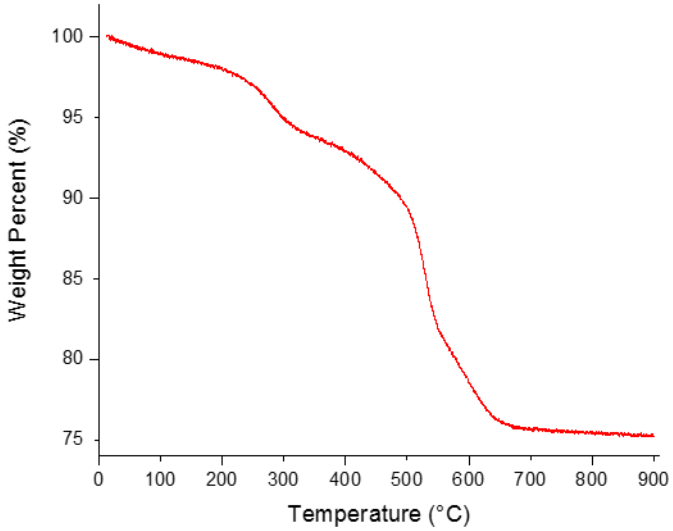

Fig. S4 TGA curve under air flow shows a weight loss of about 24.8 % this is generally consistent with that seen for zeolites.

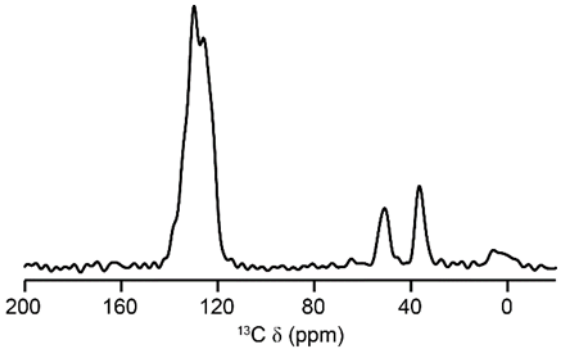

Fig. S5 ^{13}C NMR spectrum from SAZ-1 (A) showing the intact SDA is within the zeolite.

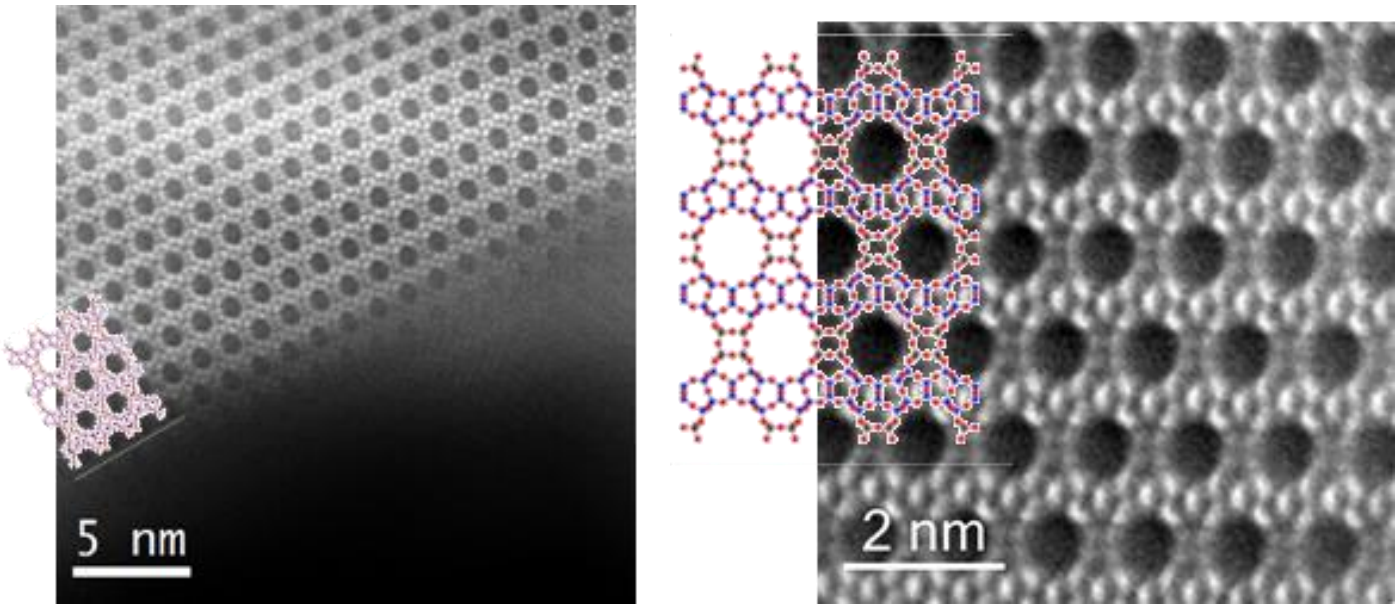

Fig. S6 A. Blown up images HADDF STEM images of SAZ-1. The 001 direction showing the presence of well ordered 14 ring pores formed by the connection of the silicate layers with D4R units

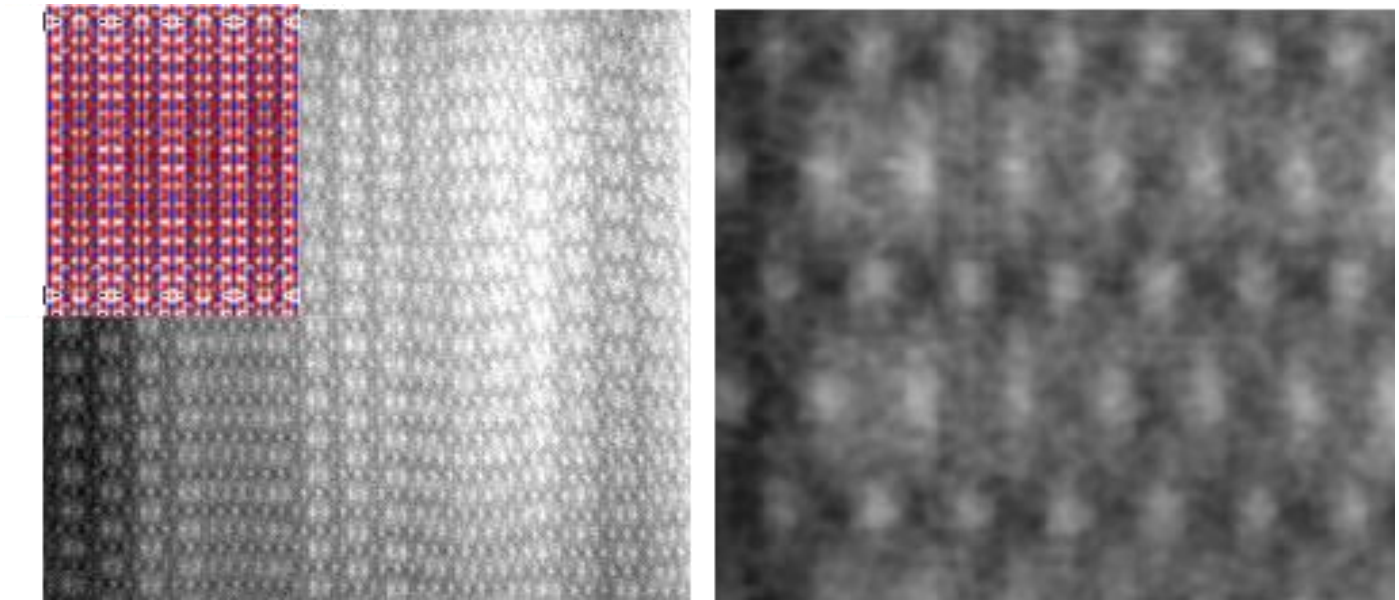

Fig. S6 B . Blown up images from HADDF STEM in the 110 direction showing the large amount of density looking through the layer and D4R units, this also shows the disorder present in this direction primarily caused defects in crystal growth.

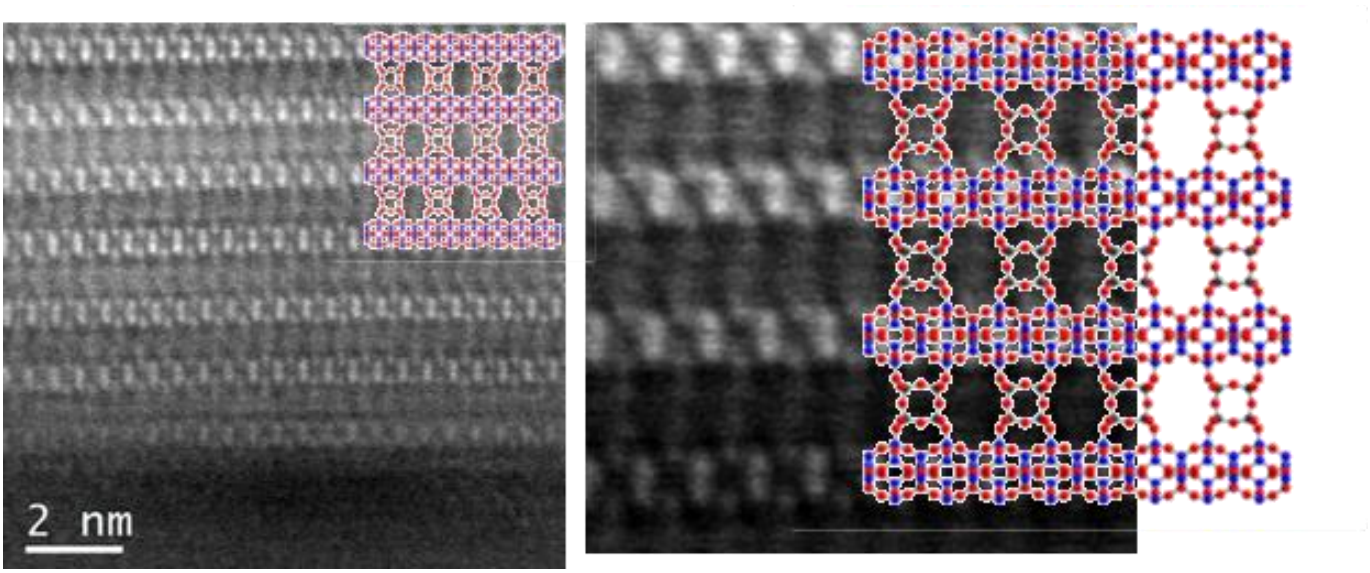

Fig. S6 C Blown up images from HADDF STEM in the 010 direction (E and F) showing the strong presence of the silicate layers, but a blurring where the 10 ring pores should be indicating the disorder present in this direction caused by the ability for the D4R linkages to be disordered in the 010 and the 100 directions as is indicated by the single analysis.

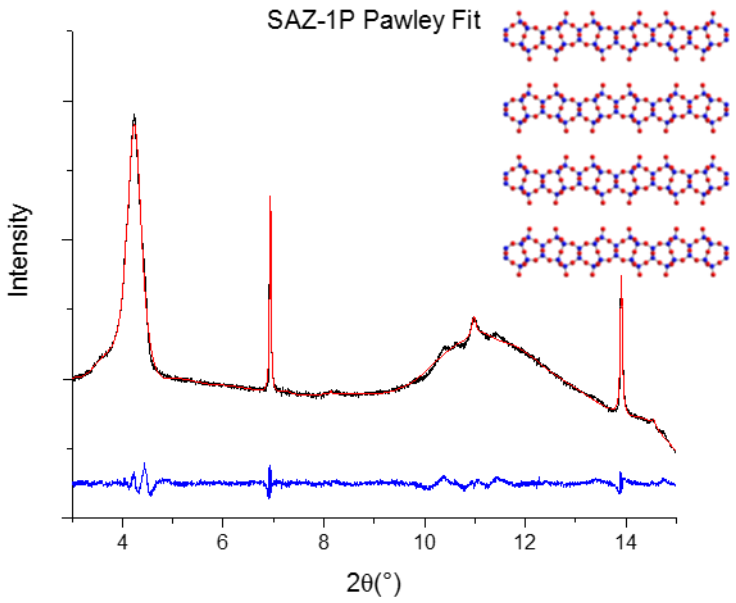

Fig. S7 Pawley refinement of SAZ-1P from synchrotron data showing the Experimental PXRD (Black), Calculated (Red) and Difference (Blue). The fit was good despite the inherent disorder expected from such a lamellar structure as SAZ-1P, which provided minimal data to refine against. The R_{wp}= 0.94 % and R_{exp}= 0.63 % for the cell C*mmm* *a*= 22.274(3), *b*= 13.6359(5) and *c*= 4.9708(6).

Table S1 Shows the surface are attained for SAZ-1 and it's derivatives. Clearly showing the loss in surface area after the disassembly of the *d4r* to form SAZ-1P, then the further loss of surface area after further reduction of the interlayer distance during the formation of the direct O-linkages and the daughter zeolite SAZ-2. The data also shows the increase in surface area as the interlayer distance is increased with the addition of *s4r* linkages between the layers and the formation of IPC-16.

Sample	Surface area (m^2/g)
SAZ-1	257.94 ±0.72
SAZ-1P	158.68 ±1.95
IPC-15	148.19 ±1.27
IPC-16	170.06 ±1.01

Fig. S8 shows the adsorption isotherms attained for SAZ1 (black), IPC-15 (red) and IPC-16 (blue).

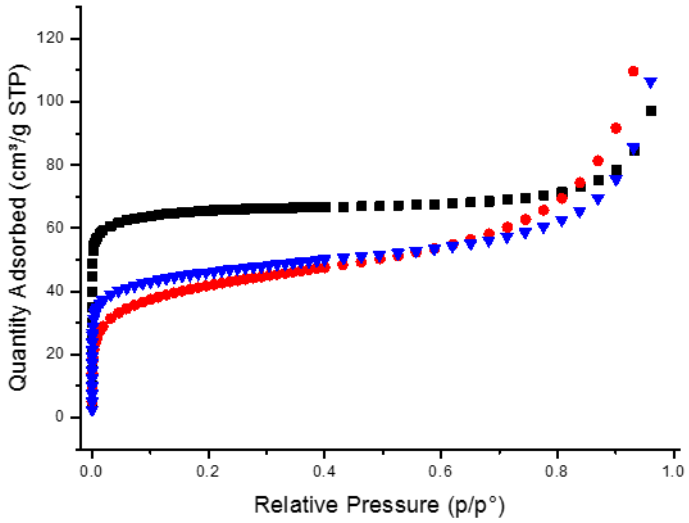

DFT Calculations

Structures of SAZ-1, IPC-15 and IPC-16 zeolites were modelled theoretically using DFT and FF methods. The DFT structures were optimized periodically without symmetry constraints using PBE1 functional with D32 dispersion energy correction and PAW approximation3 as implemented in VASP-5.3.3 program suite.4 The energy cut-off was set to 800 eV and Brillouin zone sampling was restricted to Γ-point. All structures were also optimized using Sanders-Leslie-Catlow force field5 implemented in GULP-4.0 program6, 7, both without symmetry and with highest possible symmetry for each structure. A LID criteria analysis8 has been performed on the most stable zeolite structures with P1 symmetries. All three zeolites fulfil all of the LID criteria. Furthermore, the high-symmetry structures were compared with the theoretically predicted zeolite structures in the Bronze database at hypotheticalzeolites.net.9 The Bronze database contains zeolites with maximum of six symmetry unique T sites; therefore, it is only meaningful to search IPC-15 zeolite, for which the match was indeed found (Bronze database entry 65_4_663653).

1. J. P. Perdew, K. Burke and M. Ernzerhof, Phys. Rev. Lett., 1996, 77, 3865-3868.
2. S. Grimme, J. Antony, S. Ehrlich and H. Krieg, The Journal of Chemical Physics, 2010, 132, 154104.
3. P. E. Blöchl, Phys. Rev. B, 1994, 50, 17953-17979.
4. G. Kresse and J. Hafner, Phys. Rev. B, 1993, 47, 558-561.
5. M. Sanders, M. Leslie and C. Catlow, J. Chem. Soc., Chem. Commun., 1984, 1271-1273.
6. J. D. Gale, Journal of the Chemical Society, Faraday Transactions, 1997, 93, 629-637.
7. J. D. Gale and A. L. Rohl, Molecular Simulation, 2003, 29, 291-341.

8. Y. Li, J. Yu and R. Xu, Angew. Chem. Int. Ed., 2013, 52, 1673-1677.

9. M. D. Foster and M. M. J. Tracy, A Database of Hypothetical Zeolite Structures: http://www.hypotheticalzeolites.net, 2016.